

## Miniature photoconducting capacitor array as a source for tunable THz radiation

D. Hashimshony, A. Zigler, and K. Papadopoulos

Citation: [Review of Scientific Instruments](#) **71**, 2380 (2000); doi: 10.1063/1.1150624

View online: <http://dx.doi.org/10.1063/1.1150624>

View Table of Contents: <http://scitation.aip.org/content/aip/journal/rsi/71/6?ver=pdfcov>

Published by the [AIP Publishing](#)

---

### Articles you may be interested in

[High power subterahertz electromagnetic wave radiation from GaN photoconductive switch](#)

Appl. Phys. Lett. **91**, 071112 (2007); 10.1063/1.2771528

[Generation of terahertz radiation using zinc oxide as photoconductive material excited by ultraviolet pulses](#)

Appl. Phys. Lett. **87**, 261112 (2005); 10.1063/1.2158514

[GaP THz wave generator and THz spectrometer using Cr:Forsterite lasers](#)

Rev. Sci. Instrum. **76**, 123109 (2005); 10.1063/1.2140223

[Generation and field-resolved detection of femtosecond electromagnetic pulses tunable up to 41 THz](#)

Appl. Phys. Lett. **76**, 3191 (2000); 10.1063/1.126625

[A photoconductive, miniature terahertz source](#)

Appl. Phys. Lett. **72**, 3100 (1998); 10.1063/1.121559

---



Edwards are at the forefront of vacuum  
technology for R&D and lab applications.

[Click here for product information](#)



# Miniature photoconducting capacitor array as a source for tunable THz radiation

D. Hashimshony<sup>a)</sup> and A. Zigler

*Racah Institute of Physics, The Hebrew University of Jerusalem, Jerusalem 91904, Israel*

K. Papadopoulos

*University of Maryland, College Park, Maryland 20742 and Advanced Power Inc., Washington, DC*

(Received 31 August 1999; accepted for publication 8 February 2000)

The prospects of a miniature photoconducting capacitor array as a source for THz radiation are discussed. The device consists of an alternately biased capacitor array built on a semiconductor substrate and illuminated by a short laser pulse. The laser pulse creates a propagating plasma front inside the crystal volume by side illumination, and triggers the discharging of the capacitor by shorting out the photoconducting material between each capacitor plate. The sequential discharge of the capacitor array inside the expanding plasma region can be considered as an interaction between a static wave and a superluminal ionizing front. In the present article we have demonstrated production of two cycle pulses with a center frequency of up to 1.5 THz. The device combines elements from the well-known “frozen-wave” generator and from the photoconducting switches array. The underlying physics of this radiation mechanism is very similar to the dc-to-ac conversion mechanism inside a gas-filled capacitor array which generates coherent microwave radiation.  
© 2000 American Institute of Physics. [S0034-6748(00)00506-2]

## I. INTRODUCTION

One of the growing fields of research is the spectroscopy in the THz region of the electromagnetic spectrum. The property of THz radiation, localized between infrared and microwaves, has a unique utility in characterizing electronic, vibrational, and compositional properties of solids,<sup>1-3</sup> liquids, gases,<sup>4</sup> flames,<sup>5</sup> and flows. Two main physical mechanisms have been advanced as the source of coherent THz radiation: photoconduction<sup>6</sup> and optical rectification.<sup>7,8</sup> Photoconduction relies on high-speed photoconductors generating transient current sources as radiating antennas.<sup>6,9,10</sup> The radiation is due to the large number of photocarriers created by the laser pulse and accelerated in a region of high electric field. The bandwidth of this source is usually constant and affected mainly by the internal properties of the source material and the exciting laser pulse. Optical rectification relies on a second-order nonlinear optical process induced by the presence of a dc electric field.

THz spectroscopy is usually conducted by time-resolved detection of THz pulses. With this technique, two electromagnetic pulses are sampled in the time domain, then using Fourier analysis of both pulses the frequency-dependent transmission or reflection coefficient of the sample can be obtained. The time-resolved THz spectroscopy allows an extremely broadband characterization in the relatively unexplored spectral range. The intrinsic coherency of this method enables collection of a broad range of information from the sample and automatically suppresses any incoherent background noise. It requires coherence of the sources and detec-

tor, in the sense that all pulses must have the same phase and that the detection phase can be controlled.

Lack of powerful, coherent, and tunable radiation sources in this frequency range has not permitted its extensive utilization.

A number of novel approaches have been developed recently to generate high-frequency microwaves. One approach relies on up-shifting a microwave signal by reflecting it from an optically induced ionization front moving with speed close but slower than the speed of light in a gas.<sup>11-14</sup> The underlying physics is the Doppler shift of the signal reflected by the overdense plasma front. This process has the potential for generation of short high-power radiation pulses. However, it requires a low-frequency source and results in incoherent radiation. Savage<sup>13</sup> demonstrated experimentally up-conversion of 35 GHz radiation to 116 GHz with less than 1% efficiency. Technological difficulties in producing fast laser pulses with sufficient power to generate a sharp reflecting ionization front limit both the efficiency and the upper frequency of such devices.

A number of successful experiments were conducted on a variant of this approach,<sup>15-17</sup> which generates radiation directly from a static electric field, thereby eliminating the need for an initial high-power microwave source. The static electric field of a capacitor array filled with gas and charged with alternating potentials directly converted into the emitted radiation when an ionization front crosses a capacitor, creates a burst of current and its associated half-cycle burst of radiation. The pulses radiated from each capacitor add up coherently, producing a wave train in a particular direction and frequency. The frequency and direction depend on the speed of the front, the distance, and the plasma density generated by the laser pulse. The energy of the radiated wave is

<sup>a)</sup>Electronic mail: danh@vms.huji.ac.il

provided by the electrostatic energy stored in the array. This scheme, named the dc-to-ac radiation converter (DARC), can be viewed as up-shifting radiation from zero frequency to a tunable value by the reflection from a subluminoous ionization front. The zero-frequency-wave structure resembles the well-known “frozen-wave” generator. For coherent microwave measurement, the DARC approach is very advantageous in terms of high power and coherence. The source energy comes directly from the static electric field, which is limited only by breakdown limit of the gas filling the capacitors. The spectral width of the radiation depends on the number  $N$  of capacitors and its phase can be adjusted to any value.

Experiments of the DARC concept demonstrated that the frequency can be continuously tuned between 6 and 93 GHz and generate power up to 100 W per pulse. In attempting to scale the DARC source to the THz range we are facing a number of serious difficulties.

(1) To maintain the required high voltage across the capacitors. In the original experiment, a pulsed high-voltage field was applied with a maximum of a few kV/cm at a mT pressure. Moving to the THz requires pressures approaching 1 Torr. Under these conditions, the maximum electric field that can be supported is limited to below 100 V/cm. Since the radiated power scales as  $E^2$ , the device becomes totally inefficient for frequencies above 100 GHz.

(2) The gas ionization potential is relatively high (6–10 eV). Since the radiation frequency scales linearly with the plasma frequency, stringent requirements are placed on the ionizing laser in terms of its wavelength and required energy per pulse. These requirements reduce the device efficiency.

The miniature photoconducting capacitor array (MPCA) device, whose preliminary demonstration was reported recently,<sup>18,19</sup> has been invented in order to avoid these difficulties, and thus extend the DARC operation to the THz regime. In the MPCA device, shown in Fig. 2, instead of a gas the capacitors are filled with photoconducting material, ZnSe in our case. The ionization front is created by a sweeping laser at an oblique angle to the device. As a result contrary to the DARC device, the ionization front is superluminoous. This constitutes the major physics difference between the DARC and the MPCA device. From the practical viewpoint, several of the difficulties in extending the DARC operation to the THz range are solved since: (1) The breakdown voltage for ZnSe, used in our experiment, and of GaAs, is 100 kV/cm, and even higher if a back-biased junction is used. The larger electric field that can be supported by the semiconductor improves the device efficiency by more than four orders of magnitude. (2) The energy gap (ionization energy) is between 1 and 3 eV, a factor between 2 and 5 lower than the gas. This relaxes significantly the laser requirements and improves the device efficiency. (3) For the superluminoous front, tuning of the device can be accomplished by simply changing the fluence of the ionizing laser. This controls the carrier number density, generating the radiation frequency that scales as the plasma frequency.

The MPCA mechanism can be considered to be a frozen-wave generator working inside a semiconductor plasma cloud. In such a device the laser pulse has two roles.

It generates the plasma region by side illumination and controls the discharge timing. Previously, we have demonstrated the generation of tunable far infrared-THz radiation inside the MPCA made of a ZnSe semiconductor crystal. The conversion occurs inside the volume of the semiconductor crystal by interaction with the superluminoous ionization front. The emitted radiation is tunable, its bandwidth is controllable, and the device is compatible with the standard THz setup. In this article we will discuss the operation of the MPCA as a source for THz radiation and its spectrum properties. We also will consider possibilities for power up-scaling.

## II. THEORETICAL CONSIDERATIONS

It is well known that the electromagnetic radiation reflected from a moving mirror, e.g., an overdense electron beam, is both frequency up-shifted and pulse compressed by the double Doppler factor  $(1 + U/c)/(1 - U/c)$ , where  $U$  is the velocity of the mirror. Unfortunately it is difficult to create relativistic electron beams with sufficient density to reflect high-frequency microwaves. In view of this, Semenova<sup>20</sup> and Lampe<sup>21</sup> considered reflection of electromagnetic radiation from relativistic ionization or recombination fronts. They showed that a nonzero reflection coefficient still exists and the radiation is still up-shifted and pulse compressed by the double Doppler factor. However, since contrary to a moving mirror the ionization front has no kinetic energy, the number of photons is not conserved upon reflection and the energy in the reflected pulse is much less than the incident energy. For the case of reflection by an overdense front, they found that the reflected power equals the incident power.

The principle of operation of the DARC device can be understood by considering first the interaction of a subluminoous ionization front moving with velocity  $U$  in the positive  $z$  direction, with an alternately biased capacitor array  $E = E_0 \sin(k_0 z) e_y$ . Viewing the interaction in the front frame, and assuming  $U \cong c$ , the Lorentz transformed electric field approximates an electromagnetic wave with  $\omega' \approx k'_0 c$ ,  $E'_0 \approx E_0$ , and Doppler-shifted frequency  $\omega' \approx \Gamma k'_0 U$ , where  $\Gamma = (1 - U^2/c^2)^{1/2}$  and the primes refer to quantities in the moving frame. In this frame the front is static, and the incident wave that moves in the negative  $z$  direction gives rise to a reflected and transmitted wave all at the same frequency  $\omega'$ . The analysis becomes similar to the up-shift of the frequency of electromagnetic waves mentioned above and is considered in Refs. 20 and 21. As noted in these references, the transmitted wave must satisfy the plasma dispersion relation  $k'^2 c^2 = \omega'^2 - \omega_e^2$ , where  $\omega_e^2$  is the plasma frequency which is invariant to the frame transformation. Transforming back to the laboratory frame, we find the emitted frequency as

$$\omega = \Gamma^2 k_0 U [1 - (U/c)(1 - \omega_e^2/\Gamma^2 k_0^2 U^2)^{1/2}]. \quad (1)$$

As noted above, the basic physics difference between the DARC and the MPCA devices is the fact that in the latter the ionization front is superluminoous. It is clear that reflection cannot occur at such a front since a reflected pulse cannot catch up with the superluminoous plasma front. What, in fact, happens is that instead of a reflected and a transmitted wave,

two propagating waves are generated in the plasma. Since  $U > c$ , the analysis must be performed in the laboratory frame.

There are three modes in the system. The first is the frozen wave, with zero frequency and wavelength  $k_0 = \pi/d$ , where  $d$  is the distance between the capacitors. The other two are the rightward (+) and leftward (-) propagating waves in the semiconductor plasma. They must satisfy the usual dispersion relation

$$k_{1,2}c/\omega = [+ , -] \sqrt{\epsilon \{ 1 - (\omega_e^2/\omega_{1,2}^2) [\omega_{1,2}/(\omega_{1,2} - i\gamma)] \}}^{1/2}, \quad (2)$$

where  $\epsilon$  is the dielectric constant of the semiconductor,  $\omega_e$  the plasma frequency, and the  $\gamma$  phenomenological dephasing rate. The continuity conditions require that the waves are in phase at the front. The phase of the frozen wave is simply  $k_0z$  and the phase of the radiation wave is  $kz + \omega t$ . The position of the front at time  $t$  is  $z = Ut$ , where  $U = c/\sin \theta$  and  $\theta$  is the incidence angle of the laser on the semiconductor. Equating these gives the phase continuity condition

$$\pm k_0c/\sin \theta = \omega_{1,2} + k_{1,2}c/\sin \theta. \quad (3)$$

Neglecting the leftward wave, since it never catches up with the front, and dropping the subscript from the frequency and wave number of the forward wave, we find from Eqs. (2) and (3) the relationship between the emitted frequency  $\omega$  and the other parameters as

$$(k_0c\beta - \omega)^2 - \omega^2\epsilon\beta^2 + \omega_e^2\epsilon\beta^2 \frac{\omega}{\omega - i\gamma} = 0, \quad (4)$$

where  $\beta = 1/\sin(\theta)$ ,  $k_0 = \pi/d$ , where  $d$  is the distance between the capacitors;  $\theta$  is the incidence angle of the laser;  $\epsilon$  is the dielectric constant of the semiconductor;  $\omega_e$  the plasma frequency; and  $\gamma$  the phenomenological dephasing rate. It is easy to see that in the absence of plasma, i.e.,  $\omega_e \Rightarrow 0$  (or  $\omega \gg \omega_e$ ), Eq. (4) reduces to the frozen generator one. However, for  $k_0c\beta \ll \omega$ , Eq. (4) becomes  $\omega(\omega - i\gamma) = \omega_e^2\epsilon\beta^2/(\epsilon\beta^2 - 1)$ . It is clear that for  $\omega_e \gg \gamma$  and  $\epsilon\beta^2 \gg 1$ , conditions easily fulfilled in our experiment,  $\omega$  can be written as

$$\omega = \omega_e = (ne^2/\epsilon m^*)^{1/2}. \quad (5)$$

Namely, in this regime of operation of the MPCA the radiation frequency is only a function of the semiconductor carrier density, which in its turn is only a function of the energy in the ionization laser pulse. We should emphasize that the above analysis depends critically on the validity of the dispersion relation given by Eq. (2). This requires that the absorption depth  $\delta$  of the laser by the semiconductor exceed  $c/\omega_e$  ( $\delta \gg c/\omega_e$ ). Otherwise, the plasma will not support collective volume plasma modes. In the MPCA device (patent pending), this is accomplished by relying on two-photon absorption. In this case,  $\delta = 1/(\alpha I)$ , where  $I$  is the laser intensity and  $\alpha$  the two-photon absorption coefficient. The plasma density  $n$  found by balancing the production rate with the recombination rate will be given by

$$n = \alpha W^2/h\nu S^2\tau. \quad (6)$$

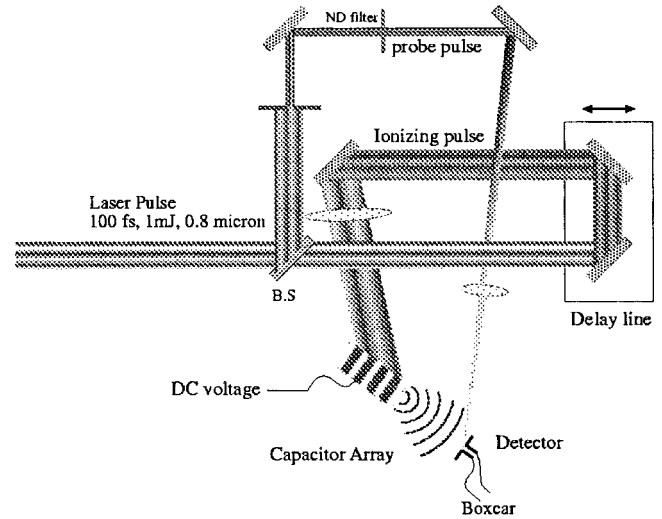


FIG. 1. Schematic diagram of the experimental setup.

In Eq. (6)  $W$  is the laser energy per pulse,  $\nu$  and  $\tau$  the laser frequency and pulse length, and  $S$  the illuminated area of the crystal. Combining Eqs. (5) and (6) we find that

$$\omega \propto W/S. \quad (7)$$

Equation (7) is an essential feature of the MPCA and states that the central frequency of the emitted radiation can be tuned by changing the incident laser fluence.

The second essential feature of the MPCA is the bandwidth control. This is accomplished by controlling the number  $N$  of active capacitors in the MPCA array. With an array of  $N$  capacitors the output pulse is  $N/2$  cycles long. For a laser pulse length  $\tau = N\pi/\omega$ , the expected bandwidth scales as

$$\Delta\omega/\omega = 2/N. \quad (8)$$

Controlling the number of active capacitors controls the bandwidth of the radiation.

Let us consider the scaling properties of the presented concept with respect to power and bandwidth. During the sweep time the electrostatic energy stored in the photoconductor is transformed into electromagnetic radiation. The energy stored in a photoconductor of length  $l$ , area  $S$  composed of capacitors occupying a fraction  $f$  of the volume with a dc field  $E_0$  is given by  $E$ :

$$E = 1/2 f \epsilon \epsilon_0 E_0^2 (sl). \quad (9)$$

The discharge time  $t = l/V_g$ , where  $V_g$  is the group velocity of the radiation. Approximating  $1/2 f \epsilon$  by unity, we find that the maximum power density  $P$  will be given by

$$P \approx 10^5 (V_g/c) E_0 / [10 \text{ kV/cm}] \text{ W/cm}^2. \quad (10)$$

This power scaling shows clearly the potential for producing high-power radiation.

### III. EXPERIMENT

An experiment was conducted to verify the theoretical results discussed above. The experimental configuration is shown in Fig. 1. It has three components. The photoconductor-based, electrically biased, radiating structure; a

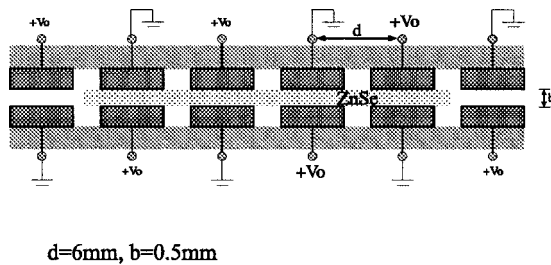


FIG. 2. Geometry of the MPCA.

Ti:sapphire 100 fs laser; and a miniature optically gated dipole antenna deposited on a silicon on sapphire (SOS) substrate, used as the radiation detector. The ZnSe crystal was chosen so that its energy gap (2.4 eV) is larger than the energy of the single photon of the laser. As a result, the carrier generation involves two photons and the absorption depth is intensity dependent. This allows for deeper penetration of the radiation so that  $\delta \gg c/\omega_e$ . The crystal was placed between the two thin glass plates, as shown in Fig. 2, with a multiple-electrode structure made by deposition of an Al line on the plates. The capacitor plates were 3 mm by 10 mm, separated by a distance of 3 mm. Thus, the initial static-wave wavelength spectrum was centered at 9 mm. The total number of active capacitors was 4, so the array contained only two static waves. The total length of the active array was 21 mm. This structure size allowed easy construction of the device without the need for microscopic lithography. Much smaller devices containing a few tens of capacitors were produced using lithographic techniques and will be presented elsewhere.

The capacitor plates were extended over the crystal, in a direction perpendicular to the radiation propagation direction, to keep the electric field inside each capacitor as uniform as possible. Two more capacitors were mounted in the array but without any photoconducting material inside them (see Fig. 2). The reason for that structure was to keep the electric field as close to zero as possible at the ends of the active array. The four capacitors were alternately biased with a voltage of 50 V to form a frozen-wave configuration. The THz radiation was generated by sweeping of a 100 fs laser pulse at an oblique angle of incidence on the crystal. The energy of the Ti:sapphire laser operated at a  $0.8 \mu$  wavelength was limited to 1 mJ at a repetition rate of 10 Hz. The wave form of the radiated electric field was measured using the standard pump and probe technique. The laser beam was split into two beams. The main beam carrying more than 95% of the energy served as the pump beam and the second beam served as the probe beam. The main beam was focused by a cylindrical lens on the side of the crystal to form the propagating ionizing front. The crystal was placed at a  $20^\circ$  angle to the pump laser beam front. The amplitude of the radiated electric field was monitored by a gated planar dipole antenna.<sup>22</sup> The initial optical path of both beams was adjusted so that both beams will reach the detector at the same time. The dipole antenna was constructed on a heavily ion-implanted silicon layer of a SOS wafer. The implantation was performed using a  $10^{15} \text{ cm}^{-2}$  dose of 100 keV  $\text{O}^+$  ions and resulted in a subpicosecond temporal response<sup>23</sup> due to

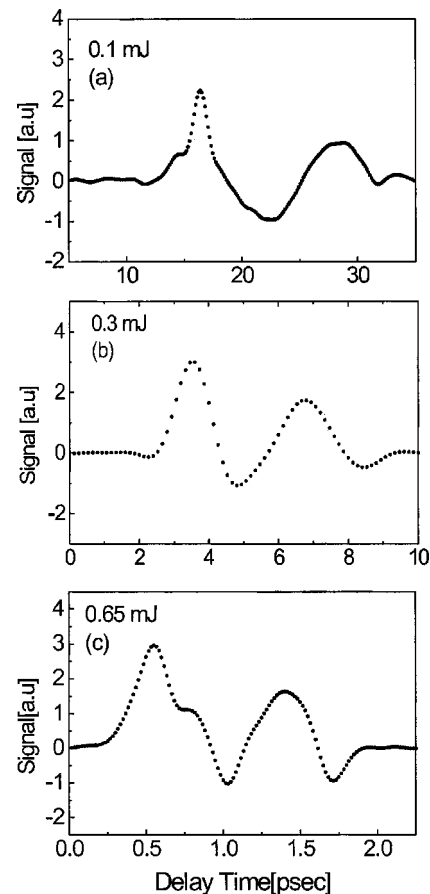


FIG. 3. Measured signal for laser energy of (a) 0.1 mJ, (b) 0.3 mJ, and (c) 0.65 mJ.

reduction of the recombination time. The antenna detector was gated at different delay times by varying the optical delay between the pump and probe laser pulses. The antenna was driven by the radiation from the capacitor array. The amplitude of the induced, time-dependent voltage across the gap was determined by measuring the average current produced in the antenna circuit. This current flows through the detector only when the gap is irradiated and shorted by the delayed 100 fs laser probe beam. An SRS250 boxcar integrator was used to collect the short current pulses. The current was averaged over many pulses until additional averaging did not change the moving average value by more than 3%. The maximum number of averaged pulses was 10 000, limited only by the integrator. This results in an averaging of 100–10 000 pulses for a delay stop. A full scan contained about 120 delay points (the number of points and the sampling resolution were predetermined by the expected emission frequency and the corresponding Nyquist frequency). As a result, a full scan lasted from 30 to 180 min. The profile of the radiation electric field was determined by monitoring the averaged current versus the time delay between the pump laser beam and the probe laser beam. The repetition rate was limited by the laser system only. Working in a 10 Hz repetition rate made the measurement extremely sensitive to the environment conditions and long-term laser stability.

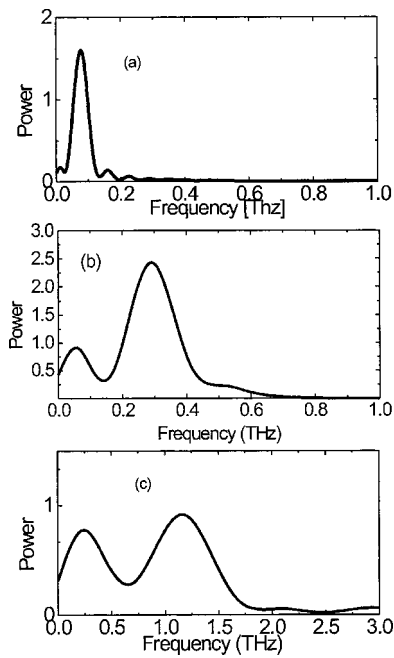


FIG. 4. Power spectrum of the signal at different laser energies.

#### IV. RESULTS

A measured temporal scan of the emitted radiation electric field for  $N=4$  is shown in Figs. 3(a)–3(c). Each scan represents the measured signal intensity versus the delay between the pump and the probe laser pulse for a certain laser power level. The delay stop was controlled mechanically by the movement of the microstage. The scan length and step size were adjusted so the full wave form could be recovered. The power spectrum profile of the corresponding signals are shown in Fig. 4. The collective nature of the interaction and the analogy with the frozen-wave generator becomes apparent by a careful examination of Fig. 3. It can be seen that the first half-cycle peak of the emitted wave form is much narrower and sharper than the following peak. A possible explanation of this effect can be that in the time-domain scan each half cycle can be considered as the footprint of one of the capacitors, where the first one to be measured in free space is the last one to be generated. The radiation created by the last capacitor is attenuated less by the transition trough the medium. The following half cycles of radiation were originally

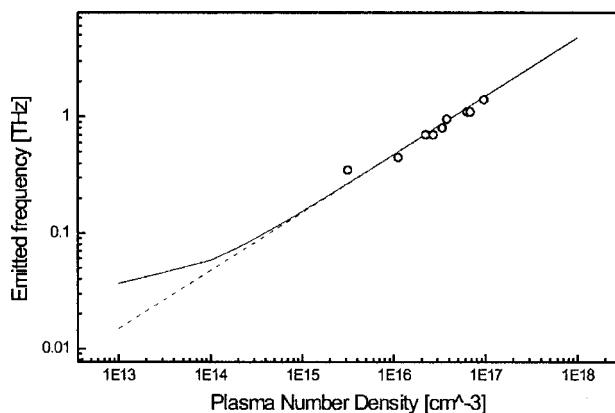


FIG. 5. Power spectrum of the signal at different laser energies.

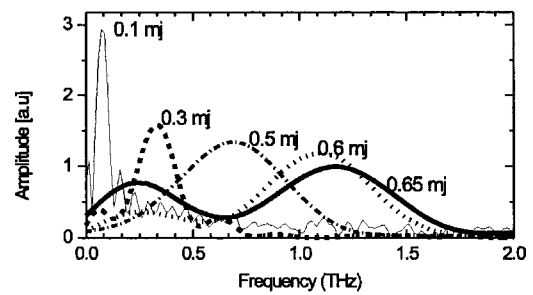


FIG. 6. Center frequency of emitted radiation (open cycle), predicted frequency (solid line), and plasma frequency (dashed line);  $V_s$  plasma number density.

generated deeper inside the plasma and affected more by the plasma presence. Figure 5 shows the power spectrum of the signal at different laser energies. It is clear that the relative bandwidth is almost constant. The reason for this is the fixed number of capacitors. As expected on the basis of Eq. (8),  $\Delta\omega/\omega=50\%$  is almost independent of the laser energy. Figure 6 shows the center frequency of the emitted radiation versus the computed plasma density for input laser energy in the range between 0.1 and 1 mJ. The open cycles are the experimental points, the solid line is the predicted center frequency according to Eq. (5), and the dashed line is the corresponding plasma frequency. It shows that in the energy range of our experiment, the emitted radiation is near the plasma frequency and the frequency of the radiation scales linearly with the energy in the laser pulse. As was discussed above, the carrier density generated, or equivalently, the plasma frequency, is proportional to the pulse energy.

Before closing, we should comment on the role of the phenomenological dephasing factor  $\gamma$  introduced in Eq. (1). As noted at that point, it is caused by either carrier collisions or electron–phonon interactions. We, furthermore, assumed that  $\omega_e \gg \gamma$ . An estimate of  $\gamma$  can be found from Fig. 3. We see that the amplitude of the second oscillation in all three cases is approximately 1/2 of the original, indicating that  $\gamma/\omega_e \approx 1/6$ . It is interesting that the dephasing constant scales with density as  $\sqrt{n}$  and is proportional to the laser fluence. These dephasing rates are consistent with electron–phonon interaction which produced the well-known Dawson–Oberman anomalous absorption near the plasma frequency. On the practical side, we should remark that this concept can be used also at the lower range of frequencies in conjunction with other up-shifting schemes. The use of photoconductors provides several advantages over gas media. The high-breakdown threshold allows significant energy storage and large radiated power. The small energy-band gap reduces the required ionization energy. Finally, the short recombination time allows a high-repetition rate. The concept is fully scalable and has the potential for providing powerful, tunable, coherent sources in a frequency range valuable for many spectroscopic applications.

<sup>1</sup>D. Grischkowsky, S. Keiding, M. V. Exter, and C. Fattinger, *J. Opt. Soc. Am. B* **7**, 2006 (1990).

<sup>2</sup>D. M. Mittelman, J. Cunningham, M. C. Nuss, and M. Geva, *Appl. Phys. Lett.* **71**, 16 (1997).

<sup>3</sup>B. I. Greene, P. N. Saeta, D. R. Dykaar, S. Schmitt-Rink, and S. Lien, *IEEE J. Quantum Electron.* **28**, 2302 (1992).

- <sup>4</sup>R. H. Jacobsen, D. M. Mittelman, and M. C. Nuss, *Opt. Lett.* **21**, 2011 (1996).
- <sup>5</sup>R. A. Chaville and D. Grischkowsky, *Opt. Lett.* **20**, 1646 (1995).
- <sup>6</sup>P. R. Smith, D. D. Auston, and M. C. Nuss, *IEEE J. Quantum Electron.* **24**, 25 (1988).
- <sup>7</sup>D. H. Auston, K. P. Cheung, J. A. Valdmanis, and D. A. Kleinman, *Phys. Rev. Lett.* **53**, 1555 (1984).
- <sup>8</sup>L. Xu, X.-C. Zhang, and D. H. Auston, *Appl. Phys. Lett.* **61**, 1784 (1992).
- <sup>9</sup>N. Katzenellenbogen and D. Grischkowsky, *Appl. Phys. Lett.* **58**, 222 (1991).
- <sup>10</sup>D. H. Auston, K. Cheung, and P. Smith, *Appl. Phys. Lett.* **45**, 284 (1984).
- <sup>11</sup>S. P. Kuo, *Phys. Rev. Lett.* **65**, 1000 (1990).
- <sup>12</sup>S. P. Kuo and A. Ren, *IEEE Trans. Plasma Sci.* **21**, 53 (1993).
- <sup>13</sup>R. L. Savage, R. P. Brogle, W. B. Mori, and C. Joshi, *IEEE Trans. Plasma Sci.* **21**, 5 (1993).
- <sup>14</sup>X. Xu, N. Yugami, and Y. Nishida, *Phys. Rev. E* **55**, 3328 (1997).
- <sup>15</sup>W. B. Mori, T. Katsouleas, J. M. Dawson, and C. H. Lai, *Phys. Rev. Lett.* **74**, 542 (1995).
- <sup>16</sup>C. H. Lai, R. Liou, and T. C. Katsouleas, *Phys. Rev. Lett.* **77**, 4764 (1996).
- <sup>17</sup>P. Muggli, R. Liou, C. H. Lai, J. Hoffman, T. C. Katsouleas, and C. Joshi, *Phys. Plasmas* **5**, 2112 (1998).
- <sup>18</sup>D. Hashimshony, A. Zigler, and K. Papadopoulos, *Appl. Phys. Lett.* **74**, 1669 (1999).
- <sup>19</sup>D. Hashimshony, A. Zigler, and K. Papadopoulos, in *Terahertz and Gigahertz Photonics*, edited by R. J. Hwu and K. Wu (SPIE, Washington, 1999), Vol. 3795, p. 477.
- <sup>20</sup>V. I. Semenova, *Sov. Radiophys.* **10**, 599 (1967).
- <sup>21</sup>M. Lampe, E. Ott, and J. H. Walker, *Phys. Fluids* **21**, 42 (1978).
- <sup>22</sup>M. van Exter, C. Fattering, and D. Grischkowsky, *Appl. Phys. Lett.* **55**, 337 (1989).
- <sup>23</sup>F. E. Doany, D. Grischkowsky, and C. C. Chi, *Appl. Phys. Lett.* **50**, 460 (1987).